A Comparison of Range-Doppler and Wavenumber Domain SAR Focusing Algorithms

Richard Bamler

Abstract— **Focusing of SAR data requires a space-variant two-dimensional correlation. Different algorithms are compared with each other in terms of their focusing quality and their ability to handle the space-variance of the correlation kernel: the range–Doppler approach with and without secondary range compression, modified range–Doppler algorithms, and four versions of the wavenumber domain processor. The phase aberrations of the different algorithms are given in analytic form. Numerical examples are presented for Seasat and ERS-1. A novel systems theoretical derivation of the wavenumber domain algorithm is presented.**

Keywords—**Synthetic Aperture Radar (SAR) data processing, range–Doppler algorithm, wavenumber domain algorithm, secondary range compression.**

I. Introduction

PROCESSING of Synthetic Aperture Radar (SAR) data requires a two-dimensional space-variant correlation of the received echo data with the point scatterer response of the SAR data acquisition system. Both the shape and the phase history of the correlation kernel vary systematically in the across-track (range) direction; a possible variation in the along track (azimuth) direction shall not be considered here. A full two-dimensional time domain correlator can handle the space-variance, but is computationally inefficient. In order to take advantage of fast frequency domain correlation techniques several algorithms have been developed in the past that impose different approximations on the correlation kernel.

For more than a decade the range–Doppler (RD) algorithm [1] has been the basis of most precision SAR processors. Several modifications of this algorithm exist [2]–[5], the most important being the secondary range compression (SRC) [2]. RD algorithms perform azimuth focusing after Fourier transforming the range compressed SAR data in the azimuth direction.

More recently, [6]–[11], a new class of algorithms has been proposed and implemented. They are often referred to as "wavenumber domain" or "ω–k" processors and employ the full two-dimensional Fourier spectrum of the data. Seismic migration techniques [12] had stimulated the development of the ω–k algorithm. Its invention resembles the breakthrough in optical SAR processing, when it was recognized that SAR data can be focused like holograms by lenses and free-space wave propagation—a procedure technologically superior to explicit matched filtering based on the technology available at that time (see, e.g., [13]). The original ω–k algorithm [6], [7], [10] was formulated in terms of the wave equation: The relationship with traditional focusing methods was not obvious at all, which might have caused an initial scepticism against the new approach. In [9], [11] approximations of the ω–k algorithm have been derived using Fourier calculus.

In this paper a systems theoretical derivation of the ω–k algorithm in its *strict* formulation—including the Stolt interpolation [6], [7], [10], [12]—is given, without employing the wave equation reasoning. This allows a comparison of RD and ω–k algorithms with respect to the following two questions:

1. *How accurately is the focusing correlation kernel approximated?* This question is addressed by investigating the phase aberrations of the implied transfer function, i.e., of the two-dimensional Fourier transform of the kernel. In this context it is sufficient to restrict the analysis to a small range interval, in effect neglecting the space-variant nature of the problem. A similar methodology is used in [5].
2. *How well is the space-variance of the correlation kernel accounted for?* Most algorithms incorporate interpolation (also referred to as change of variables, reindexing, or grid deformation) for this purpose. This raises the question of the required accuracy of the interpolation kernel and the possible artifacts introduced by a suboptimum interpolation.

The paper is organized as follows: In Section II the assumptions and the coordinate systems used in the paper are summarized. The point scatterer response of the SAR data acquisition system is derived in Section III. In Section IV the optimum time domain focusing operator, i.e., the space-variant correlation of the raw data with the point scatterer response, is formulated. Together with the exact focusing transfer function given in Section V this will serve as the reference for rating the different algorithms. In Sections VI to X the algorithms are investigated in a unified way. Section XI briefly describes a novel aberration-free algorithm. Section XII shows experimental results for simulated point scatterer responses and Section XIII summarizes the results of the analysis. The systems theoretical derivation of the ω–k algorithm is presented in the appendix.

II. Assumptions and Notations

In order to keep the discussion and the formulas as concise as possible a few simplifying assumptions are made:

Manuscript received July 16, 1991; revised February 20, 1992.

The author is with the German Aerospace Research Establishment (DLR), German Remote Sensing Data Center, W-8031 Oberpfaffenhofen, Germany.

IEEE Log Number 9200988.

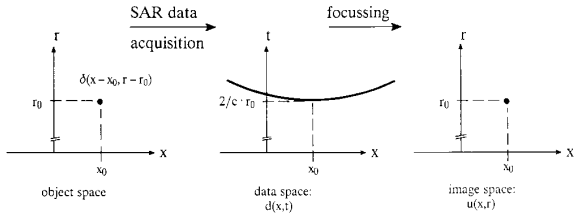

Fig. 1. Coordinate systems used in the paper.

- The sensor trajectory is a straight line.
- Earth rotation and antenna mispointing are accounted for by an effective squint angle.
- The "start–stop" approximation is adopted, i.e., no sensor movement is assumed between transmission and reception of a pulse.
- Since we are only interested in the *phase* aberrations of the processor transfer function the influences of the finite pulse bandwidth, the antenna pattern, and any window functions are not considered.
- Continuous variables will be used throughout.
- Constants are freely discarded or abbreviated.

We will use the following coordinate systems (Fig. 1):

- In the *object space* the location of scatterers is represented as a function of x (along-track or azimuth) and r (across-track or slant range).
- In the *data space* the received SAR data $d(x,t)$ are represented as a function of x and t (echo time). It is assumed that $d(x,t)$ has been already coherently demodulated and range compressed.
- The *image space* of coordinates x and r is the space of the focused (processed) complex SAR data $u(x,r)$.

III. Point Scatterer Response

SAR image formation is a two-step process: The data acquisition performs the transformation from the object space to the data space and "smears out" the energy of a single point scatterer $\delta(x-x_0, r-r_0)$ to a two-dimensional function $h(x-x_0, t; r_0)$, the *point scatterer response* (PSR). The processor tries to focus the PSR back to a single point (Fig. 1).

Let

$$p(t)\cdot\exp\{j\cdot\omega_0\cdot t\} \tag{1}$$

be the pulse transmitted by the sensor and ω_0 the carrier angular frequency. Then the echo from a scatterer a distance R away is after coherent demodulation (besides a constant)

$$p(t-2R/c)\cdot\exp\{-j\cdot\omega_0\cdot 2R/c)\}. \tag{2}$$

The pulse envelope $p(.)$ is regarded as narrow (after range compression) and will be approximated by a δ-impulse in the following. While the sensor is passing by a point scatterer located at $x=0$ and $r=r_0$ the distance R varies according to

$$R(x;r_0)=\sqrt{r_0^2+x^2}\approx r_0+\frac{x^2}{2r_0}. \tag{3}$$

The ensemble of all echoes received from the scatterer, is

$$\delta\left(t-\frac{2}{c}\cdot R(x;r_0)\right)\cdot\exp\left\{-j\omega_0\cdot\frac{2}{c}\cdot R(x;r_0)\right\}. \tag{4}$$

In the following, a normalized version of (4) will be referred to as the PSR:

$$h(x,t;r)=\delta\left(t-\frac{2}{c}\cdot\delta R(x;r)\right)\cdot\exp\left\{-j\omega_0\cdot\frac{2}{c}\cdot\delta R(x;r)\right\}. \tag{5}$$

with

$$\Delta R(x;r)=R(x;r)-r\approx x^2/(2r) \tag{6}$$

being the *range migration* (RM). The δ-line in $h(x,t;r)$ follows the RM trajectory and makes SAR processing a nonseparable two-dimensional problem. In (5) the apex of this curve has been located at the origin of the (x,t)-coordinate system; the phase of the azimuth chirp $\exp\{.\}$ has been normalized to zero for $x=0$. The parameter r accounts for the space-variance of $h(.)$ with respect to t. In the azimuth direction $h(.)$ is assumed to be space-invariant.

In the following the quadratic approximation of $\Delta R(x;r)$ from (6) will be preferred. This is sufficent for our analysis. The full hyperbolic form of $\Delta R(x;r)$ can be accounted for by all of the algorithms.

IV. Optimum Time Domain Focusing

For the purpose of comparison the "optimum" focusing of the SAR data $d(x,t)$ is taken to be the space-variant correlation with the PSR $h(.)$, i.e., a phase correction and an integration:

$$\begin{aligned}u(x,r)&=\int\int_{-\infty}^{+\infty}d(x',t)\cdot h^*(x'-x,t-2r/c;r)dx'dt\\&=\int_{-\infty}^{+\infty}d(x,t)\otimes_x h(x,t-2r/c;r)dt\end{aligned} \tag{7}$$

where the symbol "$\otimes_x$" denotes correlation in the x-direction.

Only the fact that (7) is a space-variant *and* two-dimensional operation makes SAR processing a challenge: If the RM could be neglected, i.e., $h(.)$ were effectively one-dimensional, (7) would degenerate to a set of one-dimensional correlations. If, on the other hand, only a narrow range segment around $r=r_0$ is to be focused, (7) can be replaced by a two-dimensional space-*in*variant correlation [14] followed by a change of variables from t to r:

$$u(x,r=t\cdot c/2)\approx d(x,t)\otimes_x\otimes_t h(x,t;r_0). \tag{8}$$

This approximation allows efficient SAR data focusing using two-dimensional FFT's [8], [15], [16]. Such simple algorithms, however, will not be considered here, since they do not accomodate the space-variant nature of SAR data appropriately.

Equations (7) and (8) together with (5) will serve as a reference for the following analysis. The algorithms under discussion will be judged according to how accurately they perform these operations. Whether the achieved accuracy is sufficient or not depends on the sensor parameters and on the

user's requirements. In order to gain an idea of the phase aberrations introduced by different algorithms, numerical values will be given for the Seasat and the ERS-1 cases. A slant range of 850 km±20 km and an effective squint angle corresponding to a Doppler centroid of 1500 Hz and 8000 Hz, respectively, are assumed. The processed Doppler bandwidth is 1200 Hz.

V. The Exact Transfer Function

To judge the focusing quality at one specific range $r = r_0$ the space-invariant formulation of (8) is sufficient. Taking Fourier transforms of (8) with respect to x, r, and t gives

$$U(k_x, k_r = 2\omega/c) \approx D(k_x, \omega) \cdot H^*(k_x, \omega; r_0) \tag{9}$$

where capital letters denote two-dimensional Fourier transforms; k_x and k_r are the x- and r-wavenumbers (spatial angular frequencies), respectively, and ω is the time frequency. k_x will be referred to also as the *Doppler wavenumber* in the following. It is related to the Doppler frequency f_D and the sensor velocity v via $f_D = v \cdot k_x/(2\pi)$.

$H^*(k_x, \omega; r_0)$ is the optimum transfer function for focusing points located at a constant range of $r = r_0$. This transfer function can be easily obtained by Fourier transforming $h(x, t; r_0)$ of (5): A transform in the t-direction gives

$$\exp\{-j(\omega + \omega_0) \cdot 2\Delta R(x; r)/c\}.$$

A second transform in the x-direction, using the principle of stationary phase, results in (see also [11], [16], [17]):

$$\begin{aligned} H^*(k_x, \omega; r_0) &= A_1 \cdot \exp\left\{ j \cdot r_0 \cdot \left[\sqrt{\left(\frac{\omega+\omega_0}{c/2}\right)^2 - k_x^2} - \frac{\omega+\omega_0}{c/2} \right] \right\} \\ &\approx A_1 \cdot \exp\left\{ -j \cdot r_0 \cdot \frac{c}{4} \cdot \frac{k_x^2}{\omega+\omega_0} \right\} \end{aligned} \tag{10}$$

with

$$A_1 = \sqrt{\frac{\pi \cdot c \cdot r}{j \cdot (\omega + \omega_0)}}.$$

A_1 is a slowly varying function of ω, which will be approximated here by a constant. An interesting property of $H^*(.)$ is that the range r_0 shows up as a proportional constant in the phase. This allows to cascade the transfer functions and to focus "forth and back," a procedure often referred to as "field continuation" [6], [7], [10] or "back propagation."

VI. Range-Doppler Algorithm

The RD approach works in the (k_x, t)-domain and consists of two steps:

1. *RM correction* is performed as a k_x-dependent time shift by:

$$\begin{aligned} \Delta t(k_x; r) &= \frac{2}{c} \cdot r \cdot \left(1 - \frac{1}{\sqrt{1 - (k_x \cdot c/(2\omega_0))^2}} \right) \\ &\approx -\frac{c}{4} \cdot r \cdot \frac{k_x^2}{\omega_0^2}. \end{aligned} \tag{11}$$

This operation implies a time domain interpolation which can cause artifacts in the image. If the interpolation is carried out with sufficiently high precision and only a single range position r = constant is considered, RM correction is equivalent to a k_x-dependent linear phase factor in the two-dimensional Fourier domain:

$$\exp\{-j \cdot \Delta t(k_x; r) \cdot \omega\} \approx \exp\left\{ j \cdot r \cdot \frac{c}{4} \cdot \frac{k_x^2}{\omega_0^2} \cdot \omega \right\}. \tag{12}$$

2. After RM correction a one-dimensional filter function is applied for *azimuth compression*

$$\begin{aligned} &\exp\left\{ j \cdot r \cdot \sqrt{\left(\frac{\omega_0}{c/2}\right)^2 - k_x^2} - \frac{\omega_0}{c/2} \right\} \\ &\qquad \approx \exp\left\{ -j \cdot r \cdot \frac{c}{4} \cdot \frac{k_x^2}{\omega_0} \right\}. \end{aligned} \tag{13}$$

The overall two-dimensional *transfer function* implicit to the RD approach is finally found as the product of (12) and (13) (within the quadratic approximation):

$$\exp\left\{ -j \cdot r \cdot \frac{c}{4} \cdot \frac{k_x^2}{\omega_0^2} \cdot (\omega_0 - \omega) \right\}. \tag{14}$$

A comparison between this equation and the exact transfer function from (10) shows that the RD algorithm introduces a two-dimensional phase aberration of

$$\begin{aligned} &\exp\left\{ -j \cdot r \cdot \frac{c}{4} \cdot k_x^2 \cdot \left(\frac{\omega_0 - \omega}{\omega_0^2} - \frac{1}{\omega + \omega_0} \right) \right\} \\ &\qquad = \exp\left\{ j \cdot r \cdot \frac{c}{4} \cdot \frac{k_x^2}{\omega_0^2} \cdot \frac{\omega^2}{\omega + \omega_0} \right\}. \end{aligned} \tag{15}$$

For high Doppler wavenumbers k_x, i.e., highly squinted SAR's, this term causes defocusing in the range direction. For the Seasat and the ERS-1 cases mentioned in Section IV the maximum values for k_x are 1.86 m^{-1} and 7.61 m^{-1}, respectively. The maximum quadratic phase errors at the edge of the range bandwidth are thus

$$1.56 \text{ rad} = 0.50 \cdot \pi \qquad \text{for Seasat}$$
$$0.24 \text{ rad} = 0.08 \cdot \pi \qquad \text{for ERS-1.}$$

A quadratic phase error of $\pi/4$ is usually accepted as an upper limit for good focusing quality when only detected images are considered and phase is not of concern.

The above phase aberrations can be easily corrected for, if the following approximations are justified:

1. The bandwidth of the transmitted pulse is small compared to the carrier frequency:

$$\omega + \omega_0 \approx \omega_0 \tag{16}$$

2. The Doppler wavenumber can be replaced by the Doppler centroid wavenumber k_{x0}:

$$k_x \approx k_{x0} \tag{17}$$

3. The range interval to be focused is small compared to the total range distance:

$$r \approx r_0 = \text{const.} \tag{18}$$

Then the above aberration term takes the following form:

$$\exp\left\{j \cdot r_0 \cdot \frac{c}{4} \cdot \frac{k_{x0}^2}{\omega_0^3} \cdot \omega^2\right\} \tag{19}$$

and can be eliminated, e.g., during range compression by properly adjusting the frequency modulation rate of the range reference chirp, a procedure known as *secondary range compression* (SRC) [2], [3].

The residual phase errors after SRC introduced by the approximations of (16) and (18) are below $\pi/100$ for both Seasat and ERS-1. The approximation (17), however, leaves us with a phase error of

$$0.75 \text{ rad} = 0.24 \cdot \pi \qquad \text{for Seasat}$$
$$0.03 \text{ rad} = 0.01 \cdot \pi \qquad \text{for ERS-1}$$

for the maximum Doppler frequencies to be processed. See also [3] for the case of even higher squint.

VII. Modified Range–Doppler Algorithms

A further improvement of the RD algorithm is possible by considering the residual aberrations due to the approximations (16), (18), and especially (17). In [4] an algorithm for squint imaging mode SAR (SIM SAR) is proposed that corrects the phase from (15) directly in the (k_x, ω)-domain, i.e., after a two-dimensional Fourier transform of the data.

In [3], [5] it is proposed to compensate for the aberrations during RM correction in the range–Doppler domain by using interpolation kernels, whose spectra have the desired phase behavior. By this method it is possible to adapt the SRC in both r- and k_x-directions. The cost for this adaptivity is a more complicated interpolation scheme, because several different and complex kernels have to be generated.

In summary, the RD algorithm with SRC models the two-dimensional transfer function within the validity of the approximations (16)–(18). The aberrations can be kept arbitrarily low by appropriate modifications at the cost of computing efficiency. The algorithm has the potential to consider the space-variance perfectly by updating the RM correction and the azimuth compression filter for every output sample. It is able to accomodate high Doppler centroid variations over range, even if several PRF bands are covered. Its drawback is the need of an interpolation in the (k_x, t)-domain for RM correction. If short interpolation kernels, e.g., cubic convolution, are used for this task, paired echoes of point targets will be observed in the image. However, any range resampling before detection or slant-to-ground projection can be performed within RM correction conveniently.

VIII. Wavenumber Domain Algorithm

In [6], [7], [10] an algorithm is proposed using the reasoning and the mathematics from the field of wave propagation. In the appendix it is shown that this ω–k algorithm can be derived directly from the time domain formulation of (7) without explicitely using the wave equation. From that, the basic ω–k algorithm proceeds as follows:

1. Two-dimensional Fourier transform of the data:

$$d(x,t) \rightarrow D(k_x, \omega) \tag{20}$$

2. Change of variables (Stolt mapping):

$$U(k_x, k_r) \propto D\left(k_x, \frac{c}{2} \cdot \sqrt{(k_r + 2\omega_0/c)^2 + k_x^2} - \omega_0\right) \tag{21}$$

3. Inverse two-dimensional Fourier transform:

$$U(k_x, k_r) \rightarrow u(x,r). \tag{22}$$

The algorithm proposed in [9] is in effect an ω–k algorithm, but uses a parabolic approximation of the Stolt mapping from step 2).

For implementing the Fourier transforms from steps 1) and 3) it is necessary to consider that both the echo receive time interval and the imaged range swath are highly offset from the origins of their coordinate systems. Let the echo data window be positioned around a time offset t_0 and define as the raw data:

$$d'(x,t) = d(x, t + t_0) \tag{23}$$

and the image:

$$u'(x,r) = u(x, r + r_0) \tag{24}$$

with

$$r_0 = \frac{c}{2} \cdot t_0. \tag{25}$$

Hence:

$$D'(k_x, \omega) = D(k_x, \omega) \cdot \exp\{j \cdot r_0 \cdot 2\omega/c\}. \tag{26}$$

and

$$U'(k_x, k_r) = U(k_x, k_r) \cdot \exp\{j \cdot r_0 \cdot k_r\}. \tag{27}$$

Further define the *Stolt mapping operator* $S\{.\}$ as a k_x-dependent point-by-point mapping from ω to k_r via

$$\omega = \frac{c}{2} \cdot \sqrt{(k_r + 2\omega_0/c)^2 + k_x^2} - \omega_0. \tag{28}$$

Then step 2) takes the following form:

$$U'(k_x, k_r) \propto \mathrm{S}\{D'(k_x, \omega) \cdot \exp\{-j \cdot r_0 \cdot 2\omega/c\}\} \cdot \exp\{j \cdot r_0 \cdot k_r\}. \tag{29}$$

Equation (29) can be modified in two ways to accomodate different implementations: The first phase function of (29) can be moved out of the Stolt mapping operator. Then:

$$U'(k_x, k_r) \propto \mathrm{S}\{D'(k_x, \omega)\} \cdot \exp\left\{-j \cdot r_0 \cdot \left(\sqrt{(k_r + 2\omega_0/c)^2 + k_x^2} - (k_r + 2\omega_0/c)\right)\right\}. \tag{30}$$

$$U'(k_x,k_r) \propto \mathrm{S}\left\{ D'(k_x,\omega)\cdot \exp\left\{ j\cdot r_0\cdot \left[\sqrt{\left(\frac{\omega+\omega_0}{c/2}\right)^2 - k_x^2} - \frac{\omega_0+\omega}{c/2}\right]\right\}\right\}. \tag{32}$$

This is the original version of the ω–k algorithm [6], [7], [10]. Here the raw data spectrum is multiplied by a two-dimensional phase function *after* the Stolt mapping.

A second version follows from moving the right-hand phase function from (29) *into* the Stolt operator by applying the substitution (see Appendix)

$$k_r = \sqrt{\left(\frac{\omega+\omega_0}{c/2}\right)^2 - k_x^2} - \frac{\omega_0}{c/2}. \tag{31}$$

Then equation (32), shown on the top of this page, is obtained. In this version, from which the processors proposed in [9], [11] can be derived, the data spectrum is multiplied by a phase function *prior* to Stolt mapping. Note, that this function is identical to the "exact" transfer function from (10)!

Equations (29), (30), and (32) are equivalent from the systems theoretical point of view. Henceforth, we will refer to (32) as the ω–k algorithm, because it fits better into the methodology of this paper. Obviously, the ω–k processor described by (32) first focuses all the data by using the exact transfer function tuned to $r = r_0$. The Stolt mapping takes care of the space-variance, i.e., eliminates aberration for $r \neq r_0$.

In summary, the ω–k algorithm is indeed optimum, since it is a *direct Fourier transform pendant to* (7). It uses neither of the approximations (16)–(18). The major drawback, however, is the interpolation necessary for changing the variables. This *frequency domain interpolation* is by far more critical than RM correction. It can cause shading and multiple images in the focused data. Since the ω–k processor uses a global two-dimensional Fourier representation of the data the accommodation of Doppler centroid variations in range or azimuth exceeding the margin between the processed bandwidth and the PRF needs additional effort [18].

IX. Monochromatic Wavenumber Domain Algorithm

In order to avoid the explicit Stolt mapping several approximations of the ω–k algorithm have been proposed. A most elegant solution is based on replacing the nonlinear Stolt mapping by a simple ω-independent *shift* which, in turn, is implemented in the range–Doppler domain by means of linear phase functions. By this approximation only the wavenumbers corresponding to a single frequency $\omega = 0$ are mapped correctly, hence the term "monochromatic" ω–k processor. The phase factors are applied in the range–Doppler domain either *before* [7] the data are range Fourier transformed to the (k_x,ω)-domain or *after* [11] the data have been transformed back from this domain, depending on whether (30) or (32) is adopted. In both cases, the phase factors are given by (quadratic approximation):

$$\exp\left\{ -j\cdot (r-r_0)\cdot \frac{c}{4}\cdot \frac{k_x^2}{\omega_0}\right\} \tag{33}$$

with $r = t\cdot c/2$. Although this represents a linear phase function in the r- or t-direction, it is a *quadratic* phase in k_x as well. This allows an interpretation of the monochromatic ω–k algorithm in the terminology of RD processors:

1. The exact transfer function from (10) is applied in the (k_x,ω)-domain, i.e., points at $r = r_0$, e.g., at the center of the illuminated swath, are perfectly focused.
2. After inverse Fourier transform with respect to ω, different residual azimuth compression phase filters from (33) are applied in the range–Doppler domain to compensate for the space-variant nature of the azimuth chirp.

Obviously, the algorithm performs both RM correction and azimuth compression optimally for $r = r_0$ even with highly squinted SAR geometries. For $r \neq r_0$, however, i.e., for wide swath applications, a coma-like phase aberration can be observed:

$$\exp\left\{ -j\cdot \frac{c}{4}\cdot (r-r_0)\cdot \frac{k_x^2}{\omega_0}\cdot \frac{\omega}{\omega+\omega_0}\right\} \tag{34}$$

corresponding to a residual RM of

$$\Delta r(k_x;r) = \frac{c^2}{8}\cdot (r-r_0)\cdot \frac{k_x^2}{\omega_0^2}. \tag{35}$$

This is equivalent to a linear scaling factor different for each Doppler wavenumber k_x and can cause the following image degradations:

- A residual blurring in range direction at the edges of the swath due to uncompensated RM. In our Seasat and ERS-1 examples the uncompensated RM within the 1200-Hz processed bandwidth is:

$$\pm 4.95 \text{ m for Seasat}$$
$$\pm 1.5 \text{ m for ERS-1.}$$

- If the Doppler centroid frequency is high, a range variant shift of image samples in range direction will be present, resulting in a linear scale factor slightly larger than unity. In the Seasat and ERS-1 examples this scale factor introduces a pixel misregistration at the far end of the swath of

$$6.2 \text{ m for Seasat}$$
$$10.2 \text{ m for ERS-1.}$$

The main advantage of the monochromatic ω–k algorithm is, that it needs no interpolation at all.

X. CCRS Wavenumber Domain Algorithm

In [11] a modification of the monochromatic ω–k processor is proposed. This CCRS algorithm corrects the residual RM from (35) in the range–Doppler domain. Hence, this processor needs a time domain interpolation like the RD algorithm.

Since the residual RM is very small, neither SRC nor further corrections as described in Section VII are necessary. As already mentioned, the required residual RM correction is a k_x-dependent rescaling of the data. This is equivalent to scaling the data in the (k_x, ω)-domain by the inverse scaling factor. Hence, the CCRS algorithm approximates the Stolt mapping not only by a constant shift but also by a scaling term. It can be shown that this approximation is sufficient even for high squint SAR's.

The CCRS algorithm shows an interesting similarity with the SIM SAR algorithm from [4] as briefly sketched in Section VII. Both algorithms use the (k_x, ω)- and the (k_x, t)-domains. In the CCRS approach focusing is performed in the (k_x, ω)-domain and only *residual* RM is corrected in the (k_x, t)-domain. The SIM SAR algorithm, however, follows the RD approach, i.e., performs focusing in the (k_x, t)-domain, while the (k_x, ω)-domain is only used for correction of the phase error term from (15).

XI. Chirp Scaling Algorithms

A novel algorithm for RM correction has been proposed in [19]–[22]. It uses the fact that RM shows up as a k_x-dependent range scaling factor in the range–Doppler domain. This applies both to the full RM from (11) and for the residual RM from (35). Let us assume that the SAR system transmitted linearly frequency modulated (FM) chirps and that the data were *not* range compressed before being azimuth Fourier transformed. Then the chirp scaling theorem (see, e.g., [23, pp. 203–206]) can be employed: Each range line is multiplied by a quadratic phase function in the range–Doppler domain. This causes the range chirps to be slightly altered in their FM rates and their mean frequencies. After the subsequent range compression (using the modified FM rate) the correlation maxima are displaced by an amount proportional to the mean frequency shift.

This method can be easily incorporated into RD and ω–k processors. In the latter case it approximates the strict ω–k algorithm in the same way as the CCRS approach. However, it avoids any interpolation, or in other words, it uses the entire range chirp as an interpolation kernel.

XII. Simulations

To illustrate the aberrations of the different algorithms, three point spread functions for the squinted Seasat case have been simulated: Range and azimuth cuts through the maxima of these functions are depicted in Figs. 2 and 3. The plots show the magnitude of the focused data. Matched filter weighting has been assumed, i.e., a rectangular window in range and a sinc^2 window together with a sinc^2 antenna pattern in azimuth have been applied. In particular, it is shown:

1) The optimum, i.e., aberration-free, point spread function, as it is expected from the strict ω–k algorithm, the CCRS algorithm, the monochromatic ω–k algorithm at $r = r_0$, and an ω–k processor equipped with the chirp scaling method. Also the RD algorithm with SRC approaches this focusing quality within the accuracy of the presented plots.

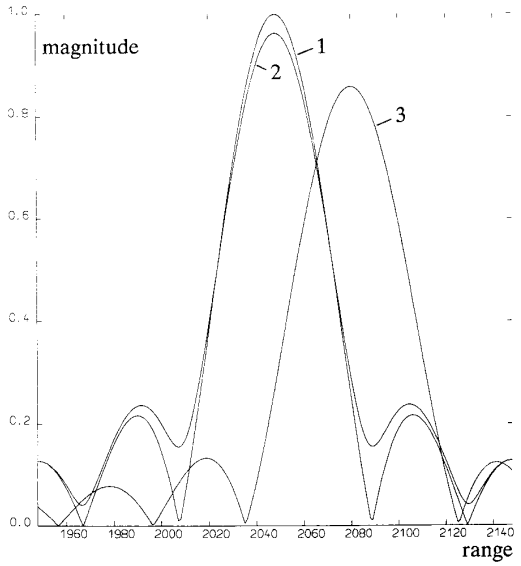

Fig. 2. Range sections of simulated point spread functions (arbitrary units), see text.

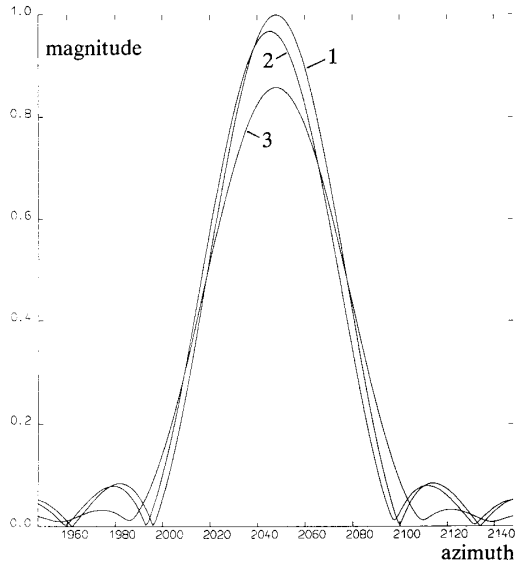

Fig. 3. Azimuth sections of simulated point spread functions (arbitrary units), see text.

2) The RD point spread function without SRC. The loss in focusing quality and the sidelobe energy increase are obvious. Also, there is a minor azimuth misregistration.
3) The point spread function of the monochromatic ω–k processor at the edge of the full swath, i.e., at $r - r_0 = 20$ km. The loss in the mainlobe energy and the range misregistration can be observed.

XIII. Conclusion

Different SAR algorithms have been compared with the direct (ideal) time domain approach. Both the RD and the

TABLE I
SUMMARY OF PHASE ABERRATIONS AND REQUIRED INTERPOLATIONS OF THE ANALYZED ALGORITHMS (ABERRATIONS ARE GIVEN AS PHASE ARGUMENTS. ONLY THE MAIN CONTRIBUTIONS WITHIN THE QUADRATIC RANGE HISTORY APPROXIMATION ARE CONSIDERED)

Algorithm	Phase Aberrations	Interpolation
RD	$r \cdot \frac{c}{4} \cdot \frac{k_x^2}{\omega_0^2} \cdot \frac{\omega^2}{\omega+\omega_0}$	time domain
RD with SRC	$r \cdot \frac{c}{4} \cdot \frac{\omega^2}{\omega_0^3} \cdot (k_x^2 - k_{x0}^2)$	time domain
RD, modified	none	time domain
RD with SRC and chirp scaling	negligible	none
ω–k, strict	none	frequency domain
ω–k, monochromatic	$-(r - r_0) \cdot \frac{c}{4} \cdot \frac{k_x^2}{\omega_0} \cdot \frac{\omega}{\omega+\omega_0}$	none
ω–k, CCRS	negligible	time domain
ω–k with chirp scaling	negligible	none

wavenumber domain algorithms have been treated in a unifying signal theoretical way. (A complementary methodology, i.e., the description of the RD processor in the terminology of the wave equation, can be found in [24]). The focusing errors of the algorithms have been quantified in terms of phase aberrations and uncompensated RM for the Seasat and in ERS-1 cases. In Table I the aberrations are summarized as well as remarks concerning the required interpolations. The well-known fact is confirmed that the conventional RD processor introduces range defocusing in images from Seasat-like sensors even at moderate squint. The gap in focusing accuracy between RD processing and the optimum ω–k algorithm is filled to a high degree by SRC, especially if this correction is adapted to the Doppler frequency. There is no evidence that a carefully designed RD processor is not as phase preserving as an ω–k processor (see also [24] for an experimental comparison).

XIV. APPENDIX

In this appendix, the ω–k algorithm will be derived from the time domain formulation of (7) using a few basic Fourier theorems applicable to space-variant operations (see also [9], [17]). The wave equation will not be used explicitly. We start from (7):

$$u(x,r) = \int_{-\infty}^{+\infty} d(x,t) \otimes_x h(x, t - 2r/c; r) dt. \tag{A1}$$

Fourier transforming with respect to x changes the correlation to a multiplication:

$$u^x(k_x,r) = \int_{-\infty}^{+\infty} d^x(k_x,t) \cdot h^{x^*}(k_x, t - 2r/c; r) dt \tag{A2}$$

where superscripts indicate Fourier transforms with respect to that variable. Parseval's theorem can now be applied to (A2) in order to transform from the t- to the ω-domain:

$$u^x(k_x,r) = \frac{1}{2\pi} \int D(k_x,\omega) \cdot H^*(k_x,\omega;r) \cdot \exp\{j \cdot 2r/c \cdot \omega\} d\omega \tag{A3}$$

where $D(.)$ and $H(.)$ are the two-dimensional spectra of $d(.)$ and $h(.)$, respectively.

Before we proceed with the derivation we calculate the Fourier transform in r-direction of the integration kernel

$$H^*(k_x,\omega;r) \cdot \exp\{j \cdot 2r/c \cdot \omega\} = A_1 \cdot \exp\left\{ j \cdot r \cdot \left[\sqrt{\left(\frac{\omega+\omega_0}{c/2}\right)^2 - k_x^2} - \frac{\omega_0}{c/2} \right] \right\}.$$

We denote its Fourier transform by $E(k_x,\omega;k_r)$:

$$E(k_x,\omega;k_r) = 2\pi \cdot A_1 \cdot \delta\left[k_r - \left[\sqrt{\left(\frac{\omega+\omega_0}{c/2}\right)^2 - k_x^2} - \frac{\omega_0}{c/2} \right] \right]. \tag{A4}$$

Note that this three-dimensional Fourier spectrum contains already the information about the "change of variables": The δ-function in $E(.)$ describes a semicircle, the two-dimensional pendant to the *Ewald sphere:*

$$k_r = \sqrt{\left(\frac{\omega+\omega_0}{c/2}\right)^2 - k_x^2} - \frac{\omega_0}{c/2} \tag{A5}$$

that is

$$\omega = \frac{c}{2}\sqrt{(k_r + 2\omega_0/c)^2 + k_x^2} - \omega_0. \tag{A6}$$

Hence $E(.)$ can be rewritten as

$$E(k_x,\omega;k_r) = 2\pi \cdot A_2 \cdot \delta\left(\omega - \frac{c}{2}\sqrt{(k_r + 2\omega_0/c)^2 + k_x^2} + \omega_0\right) \tag{A7}$$

where A_2 slightly depends on k_x and ω but will be considered as a constant here:

$$A_2 = A_1 \cdot \frac{c^2}{4} \cdot \left| \frac{k_r}{(\omega+\omega_0)} \right| \approx \text{constant}. \tag{A8}$$

With the result of (A7) we finally transform (A3) from the r- to the k_r-domain:

$$U(k_x,k_r) = A_2 \cdot \int_{-\infty}^{+\infty} D(k_x,\omega) \cdot \delta\left(\omega - \frac{c}{2} \cdot \sqrt{\cdots} + \omega_0\right) d\omega = A_2 \cdot D\left(k_x, \frac{c}{2}\sqrt{(k_r + 2\omega_0/c)^2 + k_x^2} - \omega_0\right). \tag{A9}$$

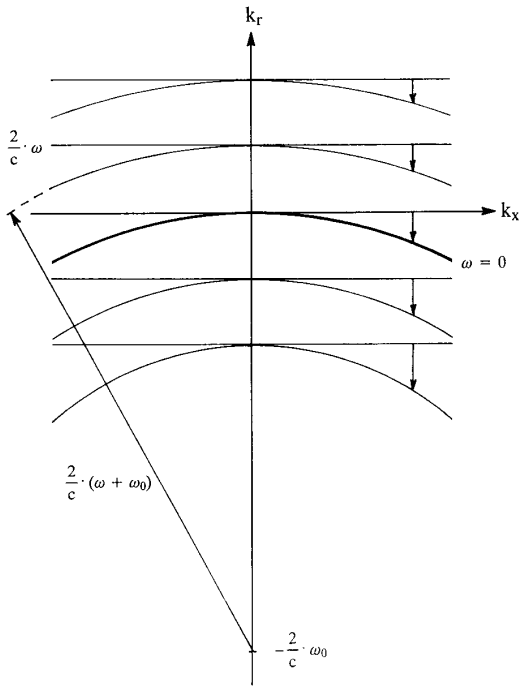

Fig. 4. Illustration of the Stolt mapping operation from ω to k_r according to equations (A5) and (A6).

This is the basic operation of the ω–k processor, the *Stolt change of variables* [12] in the two-dimensional frequency domain. It is a polychromatic extension (i.e., for $\omega \neq$ constant) of the *Fourier diffraction theorem,* well-known in the field of diffraction tomography [25]–[29]. Fig. 4 depicts the relationship between ω, k_x, k_r. Obviously, the Stolt mapping "bends" the straight lines $\omega =$ constant to arcs of circles centered at $(k_x = 0, k_r = -2\omega_0/c)$. In [9] a parabolic approximation of (A9) has been developed and referred to as "grid deformation."

ACKNOWLEDGMENT

The author appreciates interesting discussions on the subject of this paper with C. Prati, F. Rocca, R. K. Raney, P. W. Vachon and material provided by A. Smith and R. Lanari. Thanks also to H. Breit, who performed the computer simulations.

REFERENCES

[1] J. R. Bennett and I. G. Cumming, "A digital processor for the production of Seasat synthetic aperture radar imagery," in *Proc. SURGE Workshop,* Frascati, ESA-SP-154, 1979.
[2] M. Y. Jin and C. Wu, "A SAR correlation algorithm which accomodates large range migration," *IEEE Trans. Geosci. Remote Sensing,* vol. GE-22, pp. 592–597, 1984.
[3] F. H. Wong and I. G. Cumming, "Error sensitivities of a secondary range compression algorithm for processing squinted satellite SAR data, in *Proc. IGARSS '89,* Vancouver, pp. 2584–2587, 1989.
[4] C. Y. Chang, M. Jin, and J. C. Curlander, "Squint Mode SAR Processing Algorithms," in *Proc. IGARSS '89,* Vancouver, pp. 1702–1706, 1989.
[5] A. M. Smith, "A new approach to range-Doppler SAR processing," *Int. J. Remote Sensing,* vol. 12, pp. 235–251, 1991.
[6] F. Rocca, "Synthetic aperture radar: A new application for wave equation techniques," in *Stanford Exploration Project Rep.,* SEP-56, pp. 167–189, 1987.
[7] F. Rocca, C. Prati, and A. Monti Guarnieri, "New algorithms for processing of SAR data," ESA Contract Rep., ESRIN Contract no. 7998/88/F/FL(SC), 1989.
[8] G. Franceschetti and G. Schirinzi, "A SAR processor based on two-dimensional FFT codes," *IEEE Trans. Aerosp. Electron. Syst.,* vol. 26, pp. 356–366, 1990.
[9] G. Franceschetti, R. Lanari, V. Pascazio, and G. Schirinzi, "WASAR: A wide-angle SAR processor, *Proc. IEE,* Pt. F., in press.
[10] C. Cafforio, C. Prati, and F. Rocca, "SAR data focussing using seismic migration techniques," *IEEE Trans. Aerosp. Electron. Syst.,* vol. 27, pp. 199–207, 1991.
[11] R. K. Raney and P. W. Vachon, "A phase preserving SAR processor," in *Proc. IGARSS '89,* Vancouver, pp. 2588–2591, 1989.
[12] R. H. Stolt, "Migration by Fourier Transform,"*Geophysics,* vol. 43, pp. 23–48, 1978.
[13] E. N. Leith, "Range–azimuth-coupling aberrations in pulse-scanned imaging systems," *JOSA,* vol. 63, 119, 1973.
[14] R. O. Harger, *Synthetic Aperture Radar Systems: Theory and Design.* New York: Academic Press, 1970.
[15] A. DiCenco, "A new look at nonseparable synthetic aperture radar processing," *IEEE Trans. Aerosp. Electron. Syst.,* vol. 24, pp. 218–224, 1988.
[16] A. Li and O. Loffeld, "Two-dimensional SAR processing in the frequency domain," in *Proc. IGARSS '91,* Helsinki, pp. 1065–1068, 1991.
[17] R. Bamler, "A systematic comparison of SAR focussing algorithms," in *Proc. IGARSS '91,* Helsinki, pp. 1005–1009, 1991.
[18] C. Prati and F. Rocca, "Focusing SAR data with time-varying Doppler centroid," *IEEE Trans. Geosci. Remote Sensing,* vol. 30, pp. 550–559, May 1992.
[19] H. Runge and R. Bamler, "Verfahren zur Korrektur von Range-Migration bei einer Bilderzeugung bei Synthetischem Apertur Radar," DLR Patent Application, July 8, 1991.
[20] R. K. Raney, "An "exact" wide field digital imaging algorithm," submitted to *Int. J. Remote Sensing,* 1991.
[21] H. Runge and R. Bamler, "A novel high precision SAR focussing algorithm based on chirp scaling," in *Proc. IGARSS '92,* Houston, pp. 372–375, 1992.
[22] I. Cumming, F. Wong, and K. Raney, "A SAR processing algorithm with no interpolation," in *Proc. IGARSS '92,* Houston, pp. 376–379, 1992.
[23] A. Papoulis, *Systems and Transforms with Applications in Optics.* New York: McGraw-Hill, 1968.
[24] T. E. Scheuer and F. H. Wong, "Comparison of SAR processors based on a wave equation formulation," in *Proc. of IGARSS '91,* Helsinki, pp. 635–639, 1991.
[25] E. Wolf, "Three-dimensional structure determination of semi-transparent objects from holographic data," *Optics Communications,* vol. 1, pp. 153–156, 1969.
[26] R. K. Mueller, M. Kaveh, and G. Wade "Rekonstruktive tomography and applications to ultrasonics," *Proc. IEEE,* vol. 67, pp. 567–587, 1979.
[27] A. J. Devaney, "A filtered backpropagation algorithm for diffraction tomography," *Ultrasonic Imaging,* vol. 4, pp. 336–350, 1982.
[28] R. Bamler, "Diffraction and diffraction tomography: A signal theoretical description," in *Proc. Image Science '85,* Helsinki, Acta Polytechnica Scandinavica, Ph 150, pp. 281–284, 1985.
[29] R. Bamler, *Mehrdimensionale lineare Systeme: δ-Funktionen und Fourier-Transformation.* Berlin: Springer-Verlag, 1989.

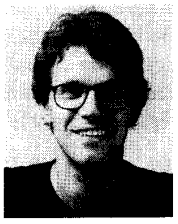

Richard Bamler received the diploma degree in electrical engineering, the Eng.Dr. degree, and the "habilitation" in the field of signal and systems theory in 1980, 1986, and 1988, respectively, from the Technical University of Munich, Germany.

He worked at that University during 1981 and 1988 on optical signal processing, wave propagation, and tomography. He is the author of a textbook on multidimensional linear systems. He joined the German Aerospace Research Establishment (DLR), Oberpfaffenhofen, in 1989, where he is currently responsible for the development of SAR algorithms for the German/Italian X-SAR experiment.